Cyclic Peptides for Lanthanide Binding

Sina Chiniforoush[1], Oksana Fizer[2], Ana de Bettencourt-Dias[2,*], David C. Cantu[1,*]

[1]Department of Chemical and Materials Engineering, University of Nevada, Reno, Reno NV, 89557, United States

[2]Department of Chemistry, University of Nevada, Reno, Reno NV, 89557, United States

*Corresponding Authors: abd@unr.edu, dcantu@unr.edu

ABSTRACT

Lanthanide ions are difficult to separate from one another due to their similar chemical properties. The discovery of lanthanide binding peptides and proteins in nature has led to an increased interest in the possibility of utilizing the strong binding of peptides to lanthanide ions for their separations; as such, there has been an effort to identify or design peptides with improved lanthanide binding and selectivity toward particular lanthanide ions. In this study, we designed lanthanide binding cyclic peptides (LBCPs) with molecular dynamics simulations, electronic structure calculations, and emission spectroscopy. Luminescent decay measurements were done to determine the number of water molecules coordinated to the Eu^{3+} ion in Eu-LBCP complexes and compare to the predicted number of water molecules by computation to assess the lanthanide binding affinity of LBCPs. Measured stability constant show binding of the LBCPs to the Eu^{3+} ion with stronger than micromolar affinity. We were able to identify multiple peptides that selectively bind to middle lanthanides. We describe the structural basis of the lanthanide-binding selectivity trend with strongest binding to the middle lanthanides, followed by the heavier lanthanides, and finally to the lighter ions.

Introduction

Rare earth elements (REEs), which include the lanthanides (Lns), have a wide range of applications in technologies such as electronics[1,2], clean energy production[3,4], energy storage[5], and bio-imaging techniques[6,7]. Despite being abundant in the earth's crust, the similarities in the physical and chemical properties of Ln ions present a challenge for their separation from each other. Current methods for extracting REEs such as hydrometallurgy[8], liquid membrane separation[9] and electrochemical separation[10] often require large amounts of resources and energy to reach the level of purity required for technological applications, and they can also produce large amounts of chemical waste that leads to deleterious environmental impacts.[8–11]

Peptides and proteins are increasingly recognized as a promising avenue for lanthanide extraction and separation.[11–16] It was shown that some organisms incorporate lanthanides and utilize them in their metabolism.[17,18] The unique coordination chemistry of Ln ions resulting from their relatively large ionic radii, their chemical hardness, and their redox inertness make them robust and versatile as Lewis acid catalysts in enzymes. The versatility of peptides, as well as their tendency to form unique structures through intramolecular interactions allows for the tuning of the coordination environment around Ln^{3+} ions, potentially increasing their selectivity toward particular Ln^{3+} ions. Moreover, peptides can be used both as chelating agents[19–22] in the liquid phase and be immobilized on solid surfaces for adsorption-based extractions.[13,23,24]

The chelation of peptides to Lns results in applications as probes to study the structure and function of biological systems. Ln^{3+} ions are used as chemical shift reagents in nuclear magnetic resonance spectroscopy and contrast agents in medical imaging,[6,25] in X-ray crystallography to increase scattering,[26,27] and in luminescence imaging techniques.[28–34]

Proteins that bind selectively to Lns have been identified in biological organisms.[35,36] Inspired by nature, Ln-binding peptides have been designed and synthesized.[11,37,38] In the present study we design lanthanide binding cyclic peptides (LBCPs), and use a combination of classical molecular dynamics (MD) simulations, density functional theory (DFT) calculations, and experimental luminescence decay measurements to characterize the lanthanide binding structure and affinity of the LBCPs. We compare the number of water molecules coordinated to the Ln^{3+} ion in Ln-peptides complex structures predicted with MD with experimentally measured values, based on the presence of OH bonds in molecules coordinated to Ln^{3+} ions that leads to non-radiative deexcitation of emissive excited states.[39,40] In addition to containing amino acid residues that are known to bind to Ln^{3+} ions with carboxylate functional groups, the peptides in this study were chosen to be small (~20 amino acids) to ensure one-to-one coordination with the Ln^{3+} ions to facilitate resolving the coordination structure. Smaller Ln-peptide complexes are more easily resolved computationally, and avoiding multiple lanthanide binding sites allows to assign spectroscopic measurements to the binding site. The peptides were cyclized with a disulfide bond between the N- and C-terminal cysteine residues to stabilize their structures.[41–43]

Methods

Computational Methods

An initial configuration of each Eu^{3+}-peptide complex was generated from the sequences of each peptide and was subjected to a series of classical molecular dynamics (MD) annealing simulations to sample a large conformational space and determine the structure of each Eu-peptide complex in water. The Eu^{3+} ion was chosen to be able to measure emission spectra and because we recently optimized the non-bonded force field parameters of the Eu^{3+} ion to bind with carboxylate and amine-containing ligands similar to peptides.[44] The starting structure for electronic structure calculations with other Ln^{3+} ions was that obtained with MD of the Eu^{3+} complex, with the Eu^{3+} ion replaced with the Ln^{3+} ion being studied. Differential binding energies of the peptides and the Nd^{3+}, Eu^{3+}, and Yb^{3+} ions were computed as the $\Delta\Delta E$ for the exchange reaction with the La^{3+} complex of the peptide as the reference (see Scheme 1) using electronic structure calculations.

Scheme 1. Exchange reaction between La^{3+} and other Ln^{3+} complexes of each peptide (PEP).

$$Ln(H_2O)_n{}^{3+} + La(H_2O)_mPEP \longrightarrow La(H_2O)_9{}^{3+} + Ln(H_2O)_xPEP + (m + n - x - 9)H_2O$$

$$\Delta\Delta E = E[Ln(H_2O)_xPEP] + E\left[La(H_2O)_9{}^{3+}\right] + (m + n - x - 9)E[H_2O] - E\left[Ln(H_2O)_n{}^{3+}\right] - E[La(H_2O)_mPEP] \quad (1)$$

The La^{3+} complex was chosen as the reference molecule as in our previous work, [45,46] and Nd^{3+}, Eu^{3+}, and Yb^{3+} as representative of the early, middle, and late lanthanides, respectively.

Identifying the Ln coordination structure in peptide complexes with molecular dynamics simulated annealing

The initial configurations of the cyclic peptides were generated from the peptide sequence using the MODPEP[47] program, which is well suited for small, cyclic peptides. All our LBCP sequences have N-terminal and C-terminal Cys residues that cyclize the peptide structure with a disulfide bond. For each peptide, one Eu^{3+} ion was inserted in the location corresponding to the center of mass for all carboxylate groups present in the peptide. The initial configurations of Eu-peptide complexes were placed at the center of a 10 nm box, and Na^+ or Cl^- counterions were added to balance the charge of the system when needed, although most peptides have a 3^- charge to compensate the Eu^{3+} charge. The geometry of the Eu-peptide complexes was minimized in gas phase followed by a 5ns NVT simulation at 363 K with a timestep of 1fs. Next, the Eu-peptide complex structure from the gas phase MD simulation the was placed at the center of a 4.5 nm box and solvated with 3800 water molecules. The water solvated Eu-peptide complex was then

subjected to a 5 ns NPT simulation to equilibrate the dimensions of the box at 1 bar and 298 K. Then, a series of NVT simulations of the system were performed in temperature windows of 363 - 313 K in decreasing 20 K temperature intervals for 1 ns each, and a final 5ns simulation at 298 K to equilibrate the structures. Finally, the resulting structure was minimized to complete the classical MD protocol.

In all MD simulations temperatures were maintained at their respective values via the velocity rescaling thermostats,[48] and for NPT simulations the pressure was maintained using the Berendsen barostat.[49] The ff14sb forcefield[50] was used for all the peptide atoms, since it has been shown to accurately predict structures for peptides and proteins.[51–53] For the Na^+ and Cl^- ions OPLS-AA parameters were used. Force field non-bonded parameters for Eu^{3+} ions were taken from our previous work, in which they were optimized to reproduce the coordination structure for Eu-EDTA.[44,46] The TIP3P water model[54] was used for the solvent. A distance cut-off of 9.0 Å was used for all non-bonded interactions. All the classical MD simulations and optimizations were performed using the GROMACS v2021[55] software.

Density functional theory calculations

The structure of each Eu-peptide complex resulting from the classical MD simulated annealing protocol, along with coordinating water molecules, were extracted to use as a starting point for further density functional theory (DFT) optimizations, replacing the Eu ion with La, Nd, or Yb. To account for the possible differences in water coordination to the Ln^{3+} ion predicted by classical force fields and DFT computations, the two closest water molecules not coordinated to the Ln^{3+} ions were also included. Due to the large size of Ln-peptide complexes, the structures were truncated in a theozyme approach where constraints are placed on outside carbon atoms to mimic the full peptide structure.[56] Figure 1 shows an example of the chosen truncated region. The atoms included in the truncation for DFT calculations were chosen primarily based on coordination (or proximity) to the Ln^{3+} ions or the presence of hydrogen bonds with coordinating amino acid residues. However, to allow for the computation of differential binding energies, for any given peptide, the choice of the truncation scheme was the same for all Ln^{3+} ions, including all residues that bind to any of the Ln^{3+} ions studied. The coordinates of backbone carbon atoms where the structure was truncated, and the α-carbon atoms of the amino acid residues included in the structure were frozen in all optimizations so that the truncated structure is consistent with the Ln-peptide complex.

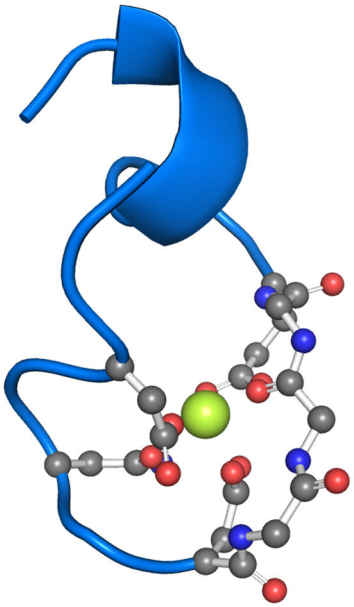

Figure 1. Structure of a Nd-peptide complex (Nd-LBT0). The truncated region chosen for DFT calculations is shown using ball-and-stick representation, and the rest of the molecule is shown in blue.

The truncated structures of the Ln-peptide complexes were optimized first using the M06[57] functional: non-Ln atoms were modeled with a 6-31G(d)[58] basis set and the Ln atoms were modeled with effective core potentials and corresponding basis sets (the Stuttgart RSC Segmented + ECP[59]). The conductor-like polarizable continuum model[60] (CPCM) was used to account for the effect of solvation by water and the D3 dispersion correction[61] was used to account for dispersion forces. Once the initial optimization was carried out, the water molecules that remained uncoordinated to the Ln^{3+} ion were removed and the structures were optimized again using the larger cc-PVTZ[62] basis set for non-Ln atoms. Single-point energy calculations were then carried out on the optimized geometries at the M06 level of theory and utilizing the DKH2 relativistic Hamiltonian:[63] the ma-DKH-def2-TZVPP basis set[64] was used for ligand and water atoms and SARC-DKH-TZVP[65] was used for Ln atoms. All DFT computations were carried out using ORCA v.50.02[66,67], and the resolution of identity chain of sphere (RIJCOSX)[68] algorithm was used for efficiency. The optimization and single point energy calculations with the levels of theory described here replicated the pK_a values of all Ln^{3+} aqua ions, and can predict experimental trends of relative binding energies of Ln-ligand complexes.[45,46,69]

Experimental Methods

Peptides were purchased from GenScript (Piscataway, NJ, USA) and from Creative Enzymes (Shirley, NY, USA) at >98% and >96% levels of purity, as determined by HPLC.

Stock 1.0 mM solutions of Eu^{3+} chloride and nitrate salts were prepared in deionized water. The exact concentrations of the Eu^{3+} salts were determined by complexometric titrations with EDTA (0.01 M) using xylenol orange as an indicator.[70]

The peptide stock solutions with an approximate concentration of 1 mM were prepared by dissolving a weighted sample of the peptide powder in 0.5 ml water. The exact concentration was determined by measuring the absorbance at 280 nm of a mixture of 20 μl of peptide sample solution in 2.0 ml of a 6 M aqueous solution of guanidine hydrochloride and using the equation below, with reported extinction coefficients of 5,685 $M^{-1}cm^{-1}$ for tryptophan, 1,285 $M^{-1}cm^{-1}$ for tyrosine, and 125 $M^{-1}cm^{-1}$ for cystine.[71]

$$\varepsilon(280)\ [M^{-1}\ cm^{-1}] = (\#Trp)(5{,}685) + (\#Tyr)(1{,}285) + (\#Cystine)(125) \quad (2)$$

To prepare Ln-peptide complexes and solutions with a resulting complex concentration of 1×10^{-5} M, known volumes of solutions of the Ln salts and of the peptide corresponding to a molar ratio of 1:1 were mixed in deionized water and stirred overnight to ensure complete binding due to the low concentrations. The resulting samples were stored at 5 °C.

The emission spectra were recorded using a Perkin Elmer LS 55 spectrometer at 25.0±0.1 °C. Eu^{3+} spectra were collected in the 500-750 nm range, with a scanning speed of 250 nm/min; slit widths for excitation and emission were set to 14 nm. In all measurements, the gain parameter was set to 900 V.

Luminescence lifetimes for Eu^{3+} were measured by monitoring its emission intensity at 616 nm on a Horiba Fluorolog spectrofluorometer at 25.0±0.1 °C using the DataStation software package, with data collected at 0.01 ms intervals over a 14 ms period following an initial 0.01 ms delay. The samples were excited at 288 nm using a xenon flash lamp, with a pulse interval of 61 ms. Excitation and emission slit widths were both set to 9 nm. Lifetimes were also measured on the Perkin Elmer LS 55, using the Short Phosphorescence Decay software package with a 0.1 ms delay, 0.1 ms time step, excitation and emission slits set at 14 nm and a 900 V gain.

The resulting decay curves were fit in Origin software to the single-exponential function below:

$$y = A_1 \exp\left(\frac{-x}{t_1}\right) + y_0 \quad (3)$$

where y is the luminescence intensity at time x after the excitation pulse, A_1 is the initial amplitude, t_1 is the luminescence lifetime, and y_0 accounts for the background signal. Measurements were done with both nitrate and chloride anions.

The number of water molecules coordinated to the Eu atom, q, was estimated based on the measured lifetimes (τ) in regular and deuterated water using the empirical equation:[72]

$$q = 1.11 \cdot (\tau_{H_2O}^{-1} - \tau_{D_2O}^{-1} - 0.31) \quad (4)$$

Stoichiometric data for complex formation in solution, along with corresponding stability constants, were determined by UV-VIS spectrophotometric titration and evaluated using SupraFit software.[73] Additional details and titration plots (Figures S1 – S3) appear in the Supporting Information (SI).

Results and Discussion

We designed a variety of lanthanide binding cyclic peptides (LBCPs) to assess their ability to strongly bind lanthanide salts in our quest to develop improved lanthanide separation systems. Our process involved computing a library of structures with the following design principles: i) cyclized with a disulfide bond for binding strength and overall stability; ii) a sequence with less than 30 amino acids for 1:1 binding following the induced fit principle; and iii) having carboxylate-containing residues with a net peptide charge of 3^- or 4^- to bind Ln^{3+} ions. We generated ~100 sequences and narrowed down the library to those peptides that had the fewest predicted water molecules in the first coordination sphere of the Eu^{3+} ion, as a quick screening metric of binding strength. An example of a peptide that was screened but not selected for further study appears in the SI.

In addition to our designed LBCPs, to test our computational approach, we also studied known baseline systems, two peptides with available structural and thermodynamic experimental data: the lanthanide binding tag reported in a study[38] by Imperiali et. al, (hereafter referred to as LBT0) and a cyclic peptide containing the sequence in the EF1 hand of lanmodulin (hereafter referred to as cEF1).[16,35] The sequences of our LBCPs, as well as those of LBT0 and cEF1, appear in Table 1.

Table 1. Sequences of the peptides investigated in this study. Lanthanide-coordinating residues (in the case of Eu^{3+} for the LBCPs) are indicated in bold.

Peptide	Sequence
LBCP1	C**E**GGRD**DD**RGGG**C**
LBCP2	CVLKLDWA**E**A**D**AAQ**D**AADLKLVC
LBCP3	CTNKNDWSES**D**SAQ**D**SS**D**NKNTC
LBCP4	CTNK**ND**WGEG**D**GAQDGG**D**NKNTC
LBCP5	CTNKNDWG**E**ADAAQ**D**AA**D**NKNTC
LBCP6	CTNKNDWS**E**A**D**AAQDAADNDKT**C**
LBT0	YI**D**T**N**N**D**GWY**E**GD**E**LLA
cEF1	C**D**P**D**K**D**GTIDLK**E**C

Structural Agreement with Experiment

To compute accurate binding energies of Ln-peptide complexes, the simulated annealing classical MD protocol needs to replicate the coordination structures of Ln-peptide complexes with high fidelity. Figure 2 shows the reported X-ray crystal structure of the Tb-LBT0 complex,[38] overlayed with the Eu-LBT0 complex predicted with MD simulation. The computed and crystal Ln-O coordination bond distances are found in Table S2. The close match between the experimental structure and the predicted structure suggests that structures found through the simulated annealing MD protocol have sufficient accuracy to serve as a good starting point for DFT computations. Although the starting point for all cyclic peptide complexes were based on MODPEP, which is well suited to predict cyclic peptides, the starting point of the Eu-LBT0 simulation was the crystal structure.

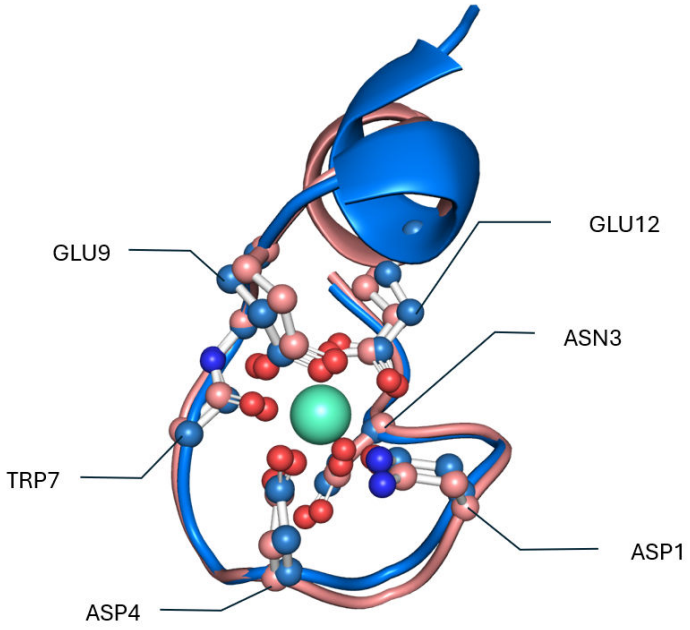

Figure 2. The X-ray crystal structure for Tb-LBT0 (blue) and computational structure (pink) for the Eu-LBT0 complexes.

To further verify our protocol, we compared cEF1 with the EF hand of lanmodulin. Table S3 shows that the residues in the EF1 hand of lanmodulin that coordinate a Nd^{3+} ion in the Nd-LanM crystal structure[16] are the same as those that coordinate the Eu^{3+} ion in a cyclic peptide that includes the same sequence (cEF1). The sequences are identical, except that cEF1 has cysteine residues at the end and beginning of the sequence to form the cyclic peptide, while EF1 is part of larger peptide (lanmodulin). The overall structural differences between the small cyclic structure of cEF1 compared with the larger lanmodulin result in Ln^{3+} coordination structure with more significant differences than those observed in Figure 2, see overlapped structures in Figure S4. However, despite these differences, EF1 and cEF1 share the identity of the Nd^{3+} coordinating amino acid residues, as well as carboxylate binding conformation (bidentate or monodentate)

same between the two structures (Table S3). This qualitative agreement in coordinating residues supports that our simulated annealing MD protocol will capture the coordination structure of small cyclic peptides to Ln^{3+} ions (the initial structure of cEF1 was predicted, not from crystal), but not the larger protein structure. Similarly, other studies have observed that the structure of acyclic form of the EF hand is different from the structure of the EF hand in lanmodulin,[74–76] showing that the loop itself will not keep the native structure.

The number of coordinated water molecules (q-values) in each Ln-LBCP complex can be used as an indirect measure of the binding strength of each peptide. Moreover, q-values are also relevant to the spectroscopic properties of these complexes, since the presence of water molecules in Ln complexes leads to fluorescence quenching. To further assess the validity of our computational protocol in describing the structures of LBCP complexes with lanthanides, we compared the number of water molecules coordinated to Eu^{3+} ions (q) in the predicted structures of the Eu-LBT0 and Eu-LBCP complexes with q-values obtained from experimentally measured luminescent decay lifetimes.[72] The results show (Table 2) that the predicted number of water molecules from computation are within the margin of error of the measured q-values for three of the six LBCPs. For LBCP1, LBCP4 and LBCP6 the measured q value is 1 to 2 water molecules higher than predicted. It is likely that we are overestimating measured q values due to the low concentration (1×10^{-5} M) that results in the presence of free Eu^{3+} ions; these are reported to be solvated with eight to nine complexed water molecules.[77–79] Further, for LBT0, computation and experiment agree within one water molecule. Also, the crystal structure of Tb-LBT0, which differs from the Eu-LBT0 solution measurements in this work, does not have any Ln-coordinated water molecules,[38] as predicted by computation.

Table 2. Predicted number of coordinated water molecules q in MD computations compared to the experimental q value. Average values and standard deviation provided when more than one measurement was performed. Emission lifetimes and individual q values appear in the Supporting Information.

	Predicted number of coordinated water molecules	**Experimental q value**
LBT0	0	0.9
LBCP1	3	5.0 ± 0.7
LBCP2	4	4.0 ± 0.8
LBCP3	5	5.7 ± 0.7
LBCP4	2	4.2 ± 0.6
LBCP5	4	3.8 ± 1.8
LBCP6	3	5.6 ± 0.4

To assess the effect of the simulation time on the structure of the complex, we ran a 5 microsecond NVT simulation of the Eu-LBCP1 complex at 363 K to ensure a larger sampling of possible conformations. While the number of coordinated water molecules fluctuated between 3

and 4, and the structure of the cyclic backbone varied, the residues coordinated to the Eu^{3+} ion remained the same as the coordinating residues found using the annealing MD protocol, as shown in Figure S5. The average number of Eu-coordinated water molecules in the 5-microsecond simulation was 3.1± 0.6. We should clarify that our simulated annealing protocol is suitable to identify the Ln^{3+} coordination structure (which did not change in the 5-microsecond simulation of Eu-LBCP1), but not the overall peptide structure (which did vary during the 5-microsecond simulation of Eu-LBCP1). Our protocol is focused on Ln^{3+} ion coordination in peptides; it is not for protein structure prediction.

Thermodynamic Agreement with Experiment

Our measured stability constants for the Eu-LBCP2, Eu-LBCP3, and Eu-LBCP4 complexes are shown in Table 3. The LBCP free energies of binding at room temperature to Eu^{3+} are in the same order of magnitude as that of Eu-LBT0 (~40 $kJ.mol^{-1}$).[38]

Table 3. Experimental stability constants of LBCPs.

Complex	Measured log*K*	Corresponding ΔG ($kJ.mol^{-1}$) at 298 K
Eu-LBCP2	6.02 ± 0.73	-34.3
Eu-LBCP3	5.08 ± 0.33	-29.0
Eu-LBCP4	5.58 ± 0.13	-31.8

Across the lanthanide series, as shown in Table 4, for Ln-LBT0 complexes, there is qualitative agreement in the relative binding energies from our calculations with measured experimental stability constants.[38] The magnitudes differ due to the absence of many interactions in the truncated analogue of the complexes, and the lack of inclusion of the entropic effects; however, the same stability trends are observed, with stronger binding of the LBT0 peptide to the Eu^{3+} ion, followed by that to Yb^{3+}, and then Nd^{3+}, all relative to the stability of the La-LBT0 complex. This trend is also observed in many of the complexes with other peptides investigated in this study. In almost all cases, the differential binding energy decreases with decreasing ionic radii, reaching a minimum for the middle lanthanides (e.g., Eu^{3+}), followed by a small increase with the later lanthanides observed with of Yb^{3+}. A similar preference for the middle lanthanides has been observed with macrocyclic ligands.[80]

Table 4. Comparison between the experimental binding free energies and computed binding energies for the, Nd, Eu, and Yb complexes with LBT0, relative to the La-LBT0 complex.

Complex	Experimental ΔΔG ($kJ.mol^{-1}$)	Computed ΔΔE ($kJ.mol^{-1}$)
La-LBT0	0.0	0.0
Nd-LBT0	-6.2	-11.1
Eu-LBT0	-9.9	-52.5

Yb-LBT0	-8.7	-41.7

To further validate our method, we computed the differential binding energies with respect to La^{3+} for additional Ln^{3+} complexes with LBT0, using the DFT-optimized geometries for La^{3+}, Nd^{3+}, Eu^{3+}, or Yb^{3+} (chosen based on proximity in size) as the initial geometry for the DFT optimization of the other Ln^{3+} complexes. As seen in Figure 3, the agreement with experiment is maintained. This includes the sharp decrease in the differential binding energies close to Eu^{3+}, and the smaller increase for later lanthanides.

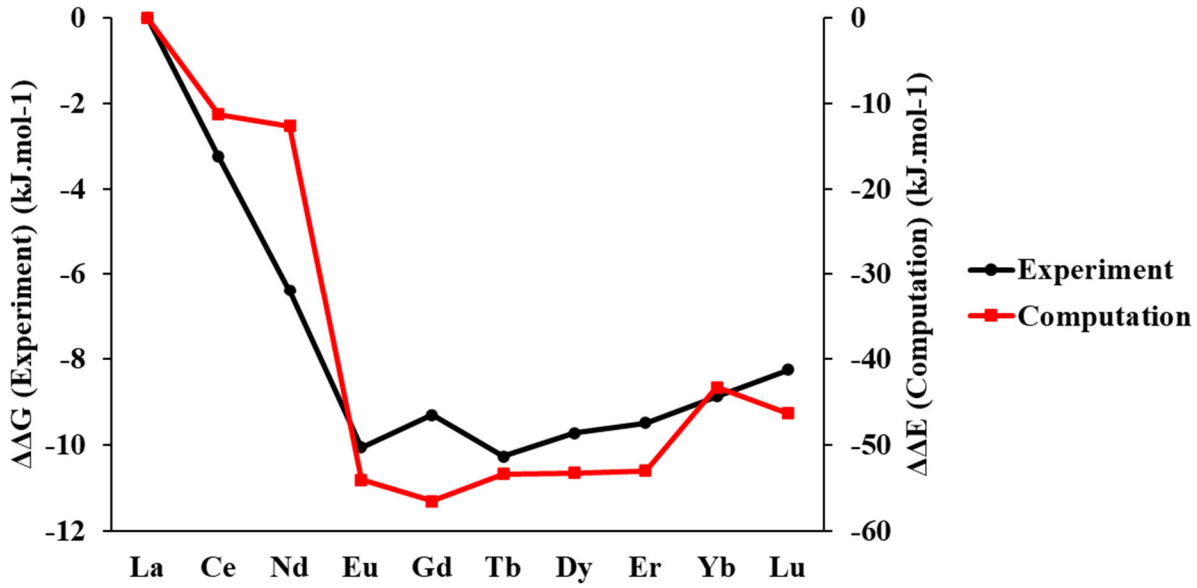

Figure 3. Differential binding energies with respect to lanthanum from experiment [38] (black) and DFT computations (red) using Scheme 1.

Coordination Structures and Binding Trends of Lanthanide Binding Cyclic Peptides

The differential binding energies (**ΔΔE)** of Nd^{3+}, Eu^{3+} and Yb^{3+} with respect to La^{3+} for each LBCP, and LBT0 as a comparison, are shown in Figure 4. The trend of the relative binding energies across the Ln^{3+} series observed with LBT0[38] is maintained most LBCPs reported in this work, with the exception LBCP1 and LBCP4. Stronger binding to the middle lanthanides than the later lanthanides can be explained as a result of a combination of two different effects. The decrease in the ionic radii of Ln^{3+} ions leads to smaller Ln-O distances, which results in an increase in electrostatic attraction. However, as the ionic radius gets smaller for the late lanthanides, steric repulsion between the coordinating residues in the peptides leads to slightly weaker binding, as in the case of Yb^{3+}.

Notably, LBCP2 and LBCP6 have stronger binding to Nd^{3+}, Eu^{3+}, and Yb^{3+} than LBT0, which suggests that the binding selectivity of LBCPs to particular Ln^{3+} ions can be improved.

The differences in trends observed for other LBCPs shows cyclic peptides are a ligand scaffold that can be tuned to change Ln-Ln selectivity.

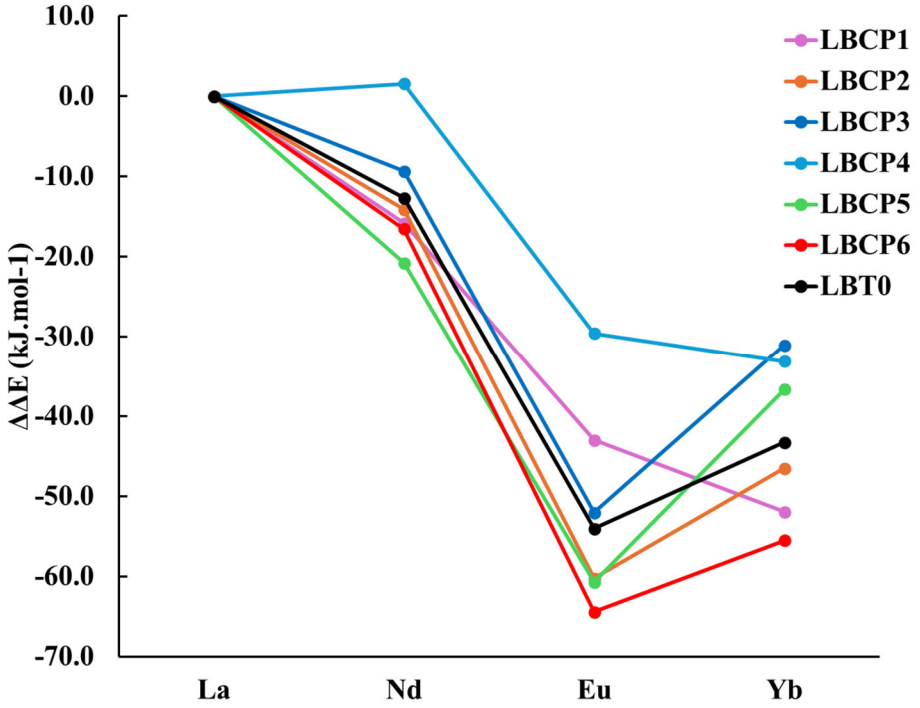

Figure 4. Differential binding energies of LBCPs, relative to the La complex of each peptide, with LBT0 as a comparison.

Table 1 includes the sequences of the LBCPs with the residues coordinated to the Ln^{3+} ions in bold; most commonly carboxylate containing residues (Asp or Glu) bind, and in some cases, C-terminal carboxylate groups and backbone amide carbonyl groups bind as well. A combination of mono- and bi-dentate carboxylate binding is also observed in the EF domains of lanmodulin.[75] Water molecules bind the Ln^{3+} ion when the peptide does not fill all Ln^{3+} binding sites. A full description of the coordinating structures of LBCPs with the Eu^{3+} ion is shown in Table 5.

Table 5. Description of the coordination structure of Eu-LBCP complexes.

Complex	Description
Eu-LBCP1	Two (2) bidentate carboxylates from Glu2, Cys13 (C-terminus). One (1) monodentate carboxylate from Asp7. Three (3) water molecules.
Eu-LBCP2	Two (2) bidentate carboxylates from Glu9, Asp11 (C-terminus). One (1) monodentate carboxylate from Asp15. Four (4) water molecules.

Eu-LBCP3	One (1) bidentate carboxylate from Asp18. Two (2) monodentate carboxylates from Asp11, Asp15. Five (5) water molecules.
Eu-LBCP4	Two (2) monodentate carboxylates from Asp6, Asp18. Three (3) backbone amides from Asp6, Asp18, Gly17. Two (2) water molecules.
Eu-LBCP5	One (1) bidentate carboxylate from Asp18. Two (2) monodentate carboxylates from Glu9, Asp15. One (1) amide from Asp15. Four (4) water molecules.
Eu-LBCP6	Three (3) bidentate carboxylates from Glu9, Asp11, Cys23 (C-terminus). Three (3) water molecules.

The Eu-LBCP5 and Eu-LBCP6 complexes (Figure 5) have the largest predicted **ΔΔE** between La and Eu, yet they display different Eu-coordination structures. While simulations predict that LBCP5 will bind the Eu^{3+} ion on the side of a helical structure with a combination of mono- and bi-dentate carboxylates, simulations predict that LCPC6 will bind the Eu^{3+} ion with three bidentate carboxylate groups. No other Eu-LBCP complex is predicted to have three bidentate carboxylate groups (Table 4), suggesting that the structural feature that results in tighter Ln^{3+} ion binding is bidentate carboxylate groups.

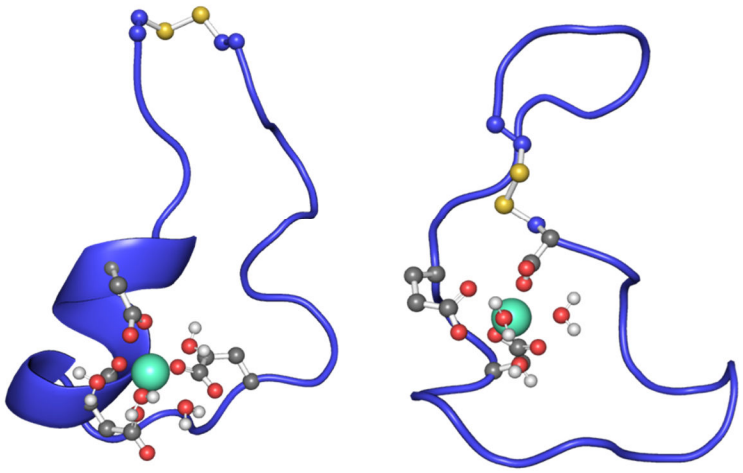

Figure 5. The predicted structure of Eu-LBCP5 (left) and Eu-LBCP6 (right) complexes.

The LBCPs presented in this work show that *de novo* designed peptides can bind lanthanide ions with sufficient binding strength to form complexes, and that selectivities to particular lanthanide ions will differ according to the lanthanide coordination structure.

Conclusion

We present lanthanide binding cyclic peptides (LBCPs) that were designed using a combination of molecular dynamics simulations, electronic structure calculations, and experimental measurements of the luminescent decay lifetimes of Eu-LBCP complexes. The computational approach can predict the structure of a previously resolved Ln-peptide complex. The predicted number of water molecules coordinated to the Ln ion in Ln-LBCP complexes agree with measured values. The measured stability constants of the LBCPs are in the same order of magnitude as previously characterized lanthanide binding peptides. Some LBCPs identified in this work are predicted to preferably bind the middle lanthanides with a selectivity similar to that of a previously known lanthanide binding tag.[38] We describe the structural basis underpinning the lanthanide-binding selectivity trend observed (middle > late > early). Although a lower number of Ln-coordinating water molecules in Ln-peptide complexes is a quick metric to assess binding strength, the Ln-peptide complexes with a higher number of bidentate carboxylate groups that coordinate the Ln ion result in stronger binding.

Acknowledgments

This material is based upon work supported by the U.S. Department of Energy, Office of Science, Office of Basic Energy Sciences, Separation Science Program, under Award Number DE-SC0024556.

Supporting Information Available

Stability constant measurement methods and titration plots (Figure S1 – S3). Example sequence not selected for further study. Table S1: Lifetimes in water and D_2O and number of coordinated water molecules (q) for Eu^{3+} complexes. Table S2: Comparison of Ln-O bond distances. Table S3: sequence of cEF1 compared with lanmodulin EF1. Figure S4. Overlap of the Nd-bound EF1 hand of lanmodulin and the Eu-bound cEF1 structure. Figure S5: the coordination structure of Eu-LBCP1 from the annealing protocol and after 5 microseconds of molecular dynamics simulation. Atomic coordinates of Eu-peptide complexes after simulated annealing. Atomic coordinates of truncated Ln-peptide complexes used for single point energy calculations.

Conflicts of interest

There are no conflicts to declare.

ORCiD

Sina Chiniforoush: 0000-0002-8428-4228

Oksana Fizer: 0000-0003-4809-3763

Ana de Bettencourt-Dias: 0000-0001-5162-2393

David C. Cantu: 0000-0001-9584-5062

References

(1) Haxel, G. B.; Hedrick, J. B.; Orris, G. J.; Stauffer, P. H.; Ii, J. W. H. Rare Earth Elements: Critical Resources for High Technology. *US Geol. Surv.* **2002**, Fact Sheet 087-02. https://doi.org/10.3133/fs08702.

(2) Haranath, D.; Mishra, S.; Joshi, A. G.; Sahai, S.; Shanker, V. Effective Doping of Rare-Earth Ions in Silica Gel: A Novel Approach to Design Active Electronic Devices. *Nano-Micro Lett.* **2011**, *3* (3), 141–145. https://doi.org/10.1007/BF03353664.

(3) Smith Stegen, K. Heavy Rare Earths, Permanent Magnets, and Renewable Energies: An Imminent Crisis. *Energy Policy* **2015**, *79*, 1–8. https://doi.org/10.1016/j.enpol.2014.12.015.

(4) Patil, A. S.; Patil, A. V.; Dighavkar, C. G.; Adole, V. A.; Tupe, U. J. Synthesis Techniques and Applications of Rare Earth Metal Oxides Semiconductors: A Review. *Chem. Phys. Lett.* **2022**, *796*, 139555. https://doi.org/10.1016/j.cplett.2022.139555.

(5) Liu, Y.; Cao, Y.; Huang, L.; Gao, M.; Pan, H. Rare Earth–Mg–Ni-Based Hydrogen Storage Alloys as Negative Electrode Materials for Ni/MH Batteries. *J. Alloys Compd.* **2011**, *509* (3), 675–686. https://doi.org/10.1016/j.jallcom.2010.08.157.

(6) Wahsner, J.; Gale, E. M.; Rodríguez-Rodríguez, A.; Caravan, P. Chemistry of MRI Contrast Agents: Current Challenges and New Frontiers. *Chem. Rev.* **2019**, *119* (2), 957–1057. https://doi.org/10.1021/acs.chemrev.8b00363.

(7) Kostelnik, T. I.; Orvig, C. Radioactive Main Group and Rare Earth Metals for Imaging and Therapy. *Chem. Rev.* **2019**, *119* (2), 902–956. https://doi.org/10.1021/acs.chemrev.8b00294.

(8) Wu, S.; Wang, L.; Zhao, L.; Zhang, P.; El-Shall, H.; Moudgil, B.; Huang, X.; Zhang, L. Recovery of Rare Earth Elements from Phosphate Rock by Hydrometallurgical Processes – A Critical Review. *Chem. Eng. J.* **2018**, *335*, 774–800. https://doi.org/10.1016/j.cej.2017.10.143.

(9) Chen, L.; Wu, Y.; Dong, H.; Meng, M.; Li, C.; Yan, Y.; Chen, J. An Overview on Membrane Strategies for Rare Earths Extraction and Separation. *Sep. Purif. Technol.* **2018**, *197*, 70–85. https://doi.org/10.1016/j.seppur.2017.12.053.

(10) Chen, Z.; Li, Z.; Chen, J.; Kallem, P.; Banat, F.; Qiu, H. Recent Advances in Selective Separation Technologies of Rare Earth Elements: A Review. *J. Environ. Chem. Eng.* **2022**, *10* (1), 107104. https://doi.org/10.1016/j.jece.2021.107104.

(11) Ye, Q.; Wang, D.; Wei, N. Engineering Biomaterials for the Recovery of Rare Earth Elements. *Trends Biotechnol.* **2024**, *42* (5), 575–590. https://doi.org/10.1016/j.tibtech.2023.10.011.

(12) Mattocks, J. A.; Cotruvo, J. A. Biological, Biomolecular, and Bio-Inspired Strategies for Detection, Extraction, and Separations of Lanthanides and Actinides. *Chem. Soc. Rev.* **2020**, *49* (22), 8315–8334. https://doi.org/10.1039/D0CS00653J.

(13) Gupta, N. K.; Gupta, A.; Ramteke, P.; Sahoo, H.; Sengupta, A. Biosorption-a Green Method for the Preconcentration of Rare Earth Elements (REEs) from Waste Solutions: A Review. *J. Mol. Liq.* **2019**, *274*, 148–164. https://doi.org/10.1016/j.molliq.2018.10.134.

(14) Ancel, L.; Niedźwiecka, A.; Lebrun, C.; Gateau, C.; Delangle, P. Rational design of lanthanide binding peptides. *Comptes Rendus Chim.* **2013**, *16* (6), 515–523. https://doi.org/10.1016/j.crci.2012.12.002.

(15) Zhang, M.; Tian, L.; Villa-Gomez, D.; Zhang, L.; Yang, W.; Liu, Y.; Cao, Y. Bio-Inspired Metal Extraction: Tailoring Peptides for Highly Selective Scandium Recovery. *Sep. Purif. Technol.* **2025**, *354*, 128640. https://doi.org/10.1016/j.seppur.2024.128640.

(16) Mattocks, J. A.; Jung, J. J.; Lin, C.-Y.; Dong, Z.; Yennawar, N. H.; Featherston, E. R.; Kang-Yun, C. S.; Hamilton, T. A.; Park, D. M.; Boal, A. K.; et al. Enhanced Rare-Earth Separation with a Metal-Sensitive Lanmodulin Dimer. *Nature* **2023**, *618* (7963), 87–93. https://doi.org/10.1038/s41586-023-05945-5.
(17) Cotruvo, J. A. Jr. The Chemistry of Lanthanides in Biology: Recent Discoveries, Emerging Principles, and Technological Applications. *ACS Cent. Sci.* **2019**, *5* (9), 1496–1506. https://doi.org/10.1021/acscentsci.9b00642.
(18) Good, N. M.; Fellner, M.; Demirer, K.; Hu, J.; Hausinger, R. P.; Martinez-Gomez, N. C. Lanthanide-Dependent Alcohol Dehydrogenases Require an Essential Aspartate Residue for Metal Coordination and Enzymatic Function. *J. Biol. Chem.* **2020**, *295* (24), 8272–8284. https://doi.org/10.1074/jbc.RA120.013227.
(19) Cisnetti, F.; Lebrun, C.; Delangle, P. A Lanthanide Binding Peptide with Short Chelating Side-Chains: Structural Impact of the Backbone Coordination. *Dalton Trans.* **2010**, *39* (15), 3560–3562. https://doi.org/10.1039/C003060K.
(20) Niedźwiecka, A.; Cisnetti, F.; Lebrun, C.; Gateau, C.; Delangle, P. Lanthanide-Binding Peptides with Two Pendant Aminodiacetate Arms: Impact of the Sequence on Chelation. *Dalton Trans.* **2012**, *41* (11), 3239–3247. https://doi.org/10.1039/C2DT11686C.
(21) Niedźwiecka, A.; Cisnetti, F.; Lebrun, C.; Delangle, P. Femtomolar Ln(III) Affinity in Peptide-Based Ligands Containing Unnatural Chelating Amino Acids. *Inorg. Chem.* **2012**, *51* (9), 5458–5464. https://doi.org/10.1021/ic300448y.
(22) Lee, H. D.; Grady, C. J.; Krell, K.; Strebeck, C.; Al-Hilfi, A.; Ricker, B.; Linn, M.; Xin, N. Y.; Good, N. M.; Martinez-Gomez, N. C.; et al. A Novel Protein for Bioremediation of Gadolinium Waste. *Protein Sci.* **2025**, *34* (4), e70101. https://doi.org/10.1002/pro.70101.
(23) Sree, H.; Swarup, G.; Gupta, S.; Pushpavanam, K. Gravity-Driven Separation for Enrichment of Rare Earth Elements Using Lanthanide Binding Peptide-Immobilized Resin. *ACS Appl. Bio Mater.* **2024**, *7* (12), 7828–7837. https://doi.org/10.1021/acsabm.3c01280.
(24) Park, D. M.; Reed, D. W.; Yung, M. C.; Eslamimanesh, A.; Lencka, M. M.; Anderko, A.; Fujita, Y.; Riman, R. E.; Navrotsky, A.; Jiao, Y. Bioadsorption of Rare Earth Elements through Cell Surface Display of Lanthanide Binding Tags. *Environ. Sci. Technol.* **2016**, *50* (5), 2735–2742. https://doi.org/10.1021/acs.est.5b06129.
(25) Moore, E. G.; Samuel, A. P. S.; Raymond, K. N. From Antenna to Assay: Lessons Learned in Lanthanide Luminescence. *Acc. Chem. Res.* **2009**, *42* (4), 542–552. https://doi.org/10.1021/ar800211j.
(26) Brodersen, D. E.; Etzerodt, M.; Madsen, P.; Celis, J. E.; Thøgersen, H. C.; Nyborg, J.; Kjeldgaard, M. EF-Hands at Atomic Resolution: The Structure of Human Psoriasin (S100A7) Solved by MAD Phasing. *Structure* **1998**, *6* (4), 477–489. https://doi.org/10.1016/S0969-2126(98)00049-5.
(27) Boggon, T. J.; Shapiro, L. Screening for Phasing Atoms in Protein Crystallography. *Structure* **2000**, *8* (7), R143–R149. https://doi.org/10.1016/S0969-2126(00)00168-4.
(28) Binnemans, K. Lanthanide-Based Luminescent Hybrid Materials. *Chem. Rev.* **2009**, *109* (9), 4283–4374. https://doi.org/10.1021/cr8003983.
(29) Armelao, L.; Quici, S.; Barigelletti, F.; Accorsi, G.; Bottaro, G.; Cavazzini, M.; Tondello, E. Design of Luminescent Lanthanide Complexes: From Molecules to Highly Efficient Photo-Emitting Materials. *Coord. Chem. Rev.* **2010**, *254* (5–6), 487–505. https://doi.org/10.1016/j.ccr.2009.07.025.

(30) Junker, A. K. R.; Hill, L. R.; Thompson, A. L.; Faulkner, S.; Sørensen, T. J. Shining Light on the Antenna Chromophore in Lanthanide Based Dyes. *Dalton Trans.* **2018**, *47* (14), 4794–4803. https://doi.org/10.1039/C7DT04788F.
(31) Barber, P. S.; De Bettencourt-Dias, A.; Johnson, K.; Monteiro, J. H. S. K. *Ligand Design in Lanthanide Complexes for Luminescence, Therapy, and Sensing*; Elsevier,Berkley,California,United States of America, 2024. https://doi.org/10.1016/bs.hpcre.2024.04.002.
(32) Monteiro, J. H. S. K.; Sobrinho, J. A.; Bettencourt-Dias, A. de. 13 Luminescence Imaging of Cancer Cells. In *Metal Ions in Bio-Imaging Techniques*; De Gruyter, 2021; pp 371–402.
(33) Stewart, O. C. Jr.; Marwitz, A. C.; Swanson, J.; Bertke, J. A.; Hartman, T.; Monteiro, J. H. S. K.; de Bettencourt-Dias, A.; Knope, K. E.; Stoll, S. L. Lanthanide Luminescence and Thermochromic Emission from Soft-Atom Donor Dichalcogenoimidodiphosphinate Ligands. *Inorg. Chem.* **2022**, *61* (39), 15547–15557. https://doi.org/10.1021/acs.inorgchem.2c02260.
(34) Monteiro, J. H. S. K.; Fetto, N. R.; Tucker, M. J.; Sigoli, F. A.; de Bettencourt-Dias, A. Carbazole-Functionalized Dipicolinato LnIII Complexes Show Two-Photon Excitation and Viscosity-Sensitive Metal-Centered Emission. *J. Lumin.* **2022**, *245*, 118768. https://doi.org/10.1016/j.jlumin.2022.118768.
(35) Cotruvo, J. A. Jr.; Featherston, E. R.; Mattocks, J. A.; Ho, J. V.; Laremore, T. N. Lanmodulin: A Highly Selective Lanthanide-Binding Protein from a Lanthanide-Utilizing Bacterium. *J. Am. Chem. Soc.* **2018**, *140* (44), 15056–15061. https://doi.org/10.1021/jacs.8b09842.
(36) Mattocks, J. A.; Ho, J. V.; Cotruvo, J. A. Jr. A Selective, Protein-Based Fluorescent Sensor with Picomolar Affinity for Rare Earth Elements. *J. Am. Chem. Soc.* **2019**, *141* (7), 2857–2861. https://doi.org/10.1021/jacs.8b12155.
(37) Webster, A. M.; Peacock, A. F. A. De Novo Designed Coiled Coils as Scaffolds for Lanthanides, Including Novel Imaging Agents with a Twist. *Chem. Commun.* **2021**, *57* (56), 6851–6862. https://doi.org/10.1039/D1CC02013G.
(38) Nitz, M.; Sherawat, M.; Franz, K. J.; Peisach, E.; Allen, K. N.; Imperiali, B. Structural Origin of the High Affinity of a Chemically Evolved Lanthanide-Binding Peptide. *Angew. Chem. Int. Ed.* **2004**, *43* (28), 3682–3685. https://doi.org/10.1002/anie.200460028.
(39) Kropp, J. L.; Windsor, M. W. Enhancement of Fluorescence Yield of Rare-Earth Ions by Heavy Water. *J. Chem. Phys.* **1963**, *39* (10), 2769–2770. https://doi.org/10.1063/1.1734096.
(40) Haas, Y.; Stein, G. Radiative and Nonradiative Pathways in Solutions. Excited States of the Europium(III) Ion. *J. Phys. Chem.* **1972**, *76* (8), 1093–1104. https://doi.org/10.1021/j100652a002.
(41) Góngora-Benítez, M.; Tulla-Puche, J.; Albericio, F. Multifaceted Roles of Disulfide Bonds. Peptides as Therapeutics. *Chem. Rev.* **2014**, *114* (2), 901–926. https://doi.org/10.1021/cr400031z.
(42) Tam, J. P.; Wong, C. T. T. Chemical Synthesis of Circular Proteins. *J. Biol. Chem.* **2012**, *287* (32), 27020–27025. https://doi.org/10.1074/jbc.R111.323568.
(43) Loo, S.; Kam, A.; Li, B. B.; Feng, N.; Wang, X.; Tam, J. P. Discovery of Hyperstable Noncanonical Plant-Derived Epidermal Growth Factor Receptor Agonist and Analogs. *J. Med. Chem.* **2021**, *64* (11), 7746–7759. https://doi.org/10.1021/acs.jmedchem.1c00551.
(44) Licup, G. L.; Summers, T. J.; Sobrinho, J. A.; de Bettencourt-Dias, A.; Cantu, D. C. Elucidating the Structure of the Eu-EDTA Complex in Solution at Various Protonation

States. *Eur. J. Inorg. Chem.* **2024**, *27* (16), e202400042. https://doi.org/10.1002/ejic.202400042.
(45) Gao, Y.; Licup, G. L.; Bigham, N. P.; Cantu, D. C.; Wilson, J. J. Chelator-Assisted Precipitation-Based Separation of the Rare Earth Elements Neodymium and Dysprosium from Aqueous Solutions. *Angew. Chem. Int. Ed.* **2024**, *63* (42), e202410233. https://doi.org/10.1002/anie.202410233.
(46) D. O'Brien, R.; J. Summers, T.; S. Kaliakin, D.; C. Cantu, D. The Solution Structures and Relative Stability Constants of Lanthanide–EDTA Complexes Predicted from Computation. *Phys. Chem. Chem. Phys.* **2022**, *24* (17), 10263–10271. https://doi.org/10.1039/D2CP01081J.
(47) Yan, Y.; Zhang, D.; Huang, S.-Y. Efficient Conformational Ensemble Generation of Protein-Bound Peptides. *J. Cheminformatics* **2017**, *9* (1), 59. https://doi.org/10.1186/s13321-017-0246-7.
(48) Bussi, G.; Donadio, D.; Parrinello, M. Canonical Sampling through Velocity Rescaling. *J. Chem. Phys.* **2007**, *126* (1), 014101. https://doi.org/10.1063/1.2408420.
(49) Berendsen, H. J. C.; Postma, J. P. M.; van Gunsteren, W. F.; DiNola, A.; Haak, J. R. Molecular Dynamics with Coupling to an External Bath. *J. Chem. Phys.* **1984**, *81* (8), 3684–3690. https://doi.org/10.1063/1.448118.
(50) Maier, J. A.; Martinez, C.; Kasavajhala, K.; Wickstrom, L.; Hauser, K. E.; Simmerling, C. ff14SB: Improving the Accuracy of Protein Side Chain and Backbone Parameters from ff99SB. *J. Chem. Theory Comput.* **2015**, *11* (8), 3696–3713. https://doi.org/10.1021/acs.jctc.5b00255.
(51) Park, J.; Lee, H.-S.; Kim, H.; Choi, J.-M. Conformational Landscapes of Artificial Peptides Predicted by Various Force Fields: Are We Ready to Simulate β-Amino Acids? *Phys. Chem. Chem. Phys.* **2023**, *25* (10), 7466–7476. https://doi.org/10.1039/D2CP05998C.
(52) Wang, X.; Xiong, D.; Zhang, Y.; Zhai, J.; Gu, Y.-C.; He, X. The Evolution of the Amber Additive Protein Force Field: History, Current Status, and Future. *J. Chem. Phys.* **2025**, *162* (3), 030901. https://doi.org/10.1063/5.0227517.
(53) Tian, C.; Kasavajhala, K.; Belfon, K. A. A.; Raguette, L.; Huang, H.; Migues, A. N.; Bickel, J.; Wang, Y.; Pincay, J.; Wu, Q.; Simmerling, C. ff19SB: Amino-Acid-Specific Protein Backbone Parameters Trained against Quantum Mechanics Energy Surfaces in Solution. *J. Chem. Theory Comput.* **2020**, *16* (1), 528–552. https://doi.org/10.1021/acs.jctc.9b00591.
(54) Jorgensen, W. L.; Chandrasekhar, J.; Madura, J. D.; Impey, R. W.; Klein, M. L. Comparison of Simple Potential Functions for Simulating Liquid Water. *J. Chem. Phys.* **1983**, *79* (2), 926–935. https://doi.org/10.1063/1.445869.
(55) Abraham, M. J.; Murtola, T.; Schulz, R.; Páll, S.; Smith, J. C.; Hess, B.; Lindahl, E. GROMACS: High Performance Molecular Simulations through Multi-Level Parallelism from Laptops to Supercomputers. *SoftwareX* **2015**, *1–2*, 19–25. https://doi.org/10.1016/j.softx.2015.06.001.
(56) Patel, H. N.; Haines, B. E.; Stauffacher, C. V.; Helquist, P.; Wiest, O. Computational Study of Base-Catalyzed Thiohemiacetal Decomposition in Pseudomonas Mevalonii HMG-CoA Reductase. *J. Phys. Chem. B* **2023**, *127* (22), 4931–4938. https://doi.org/10.1021/acs.jpcb.2c08969.
(57) Zhao, Y.; Truhlar, D. G. The M06 Suite of Density Functionals for Main Group Thermochemistry, Thermochemical Kinetics, Noncovalent Interactions, Excited States, and

Transition Elements: Two New Functionals and Systematic Testing of Four M06-Class Functionals and 12 Other Functionals. *Theor. Chem. Acc.* **2008**, *120* (1), 215–241. https://doi.org/10.1007/s00214-007-0310-x.
(58) Wiberg, K. B. Ab Initio Molecular Orbital Theory by W. J. Hehre, L. Radom, P. v. R. Schleyer, and J. A. Pople, John Wiley, New York, 548pp. (1986). *J. Comput. Chem.* **1986**, *7* (3), 379–379. https://doi.org/10.1002/jcc.540070314.
(59) Cao, X.; Dolg, M. Segmented Contraction Scheme for Small-Core Lanthanide Pseudopotential Basis Sets. *J. Mol. Struct. THEOCHEM* **2002**, *581* (1), 139–147. https://doi.org/10.1016/S0166-1280(01)00751-5.
(60) Cossi, M.; Rega, N.; Scalmani, G.; Barone, V. Energies, Structures, and Electronic Properties of Molecules in Solution with the C-PCM Solvation Model. *J. Comput. Chem.* **2003**, *24* (6), 669–681. https://doi.org/10.1002/jcc.10189.
(61) Grimme, S.; Antony, J.; Ehrlich, S.; Krieg, H. A Consistent and Accurate Ab Initio Parametrization of Density Functional Dispersion Correction (DFT-D) for the 94 Elements H-Pu. *J. Chem. Phys.* **2010**, *132* (15), 154104. https://doi.org/10.1063/1.3382344.
(62) Dunning, T. H., Jr. Gaussian Basis Sets for Use in Correlated Molecular Calculations. I. The Atoms Boron through Neon and Hydrogen. *J. Chem. Phys.* **1989**, *90* (2), 1007–1023. https://doi.org/10.1063/1.456153.
(63) Reiher, M. Relativistic Douglas–Kroll–Hess Theory. *WIREs Comput. Mol. Sci.* **2012**, *2* (1), 139–149. https://doi.org/10.1002/wcms.67.
(64) Zheng, J.; Xu, X.; Truhlar, D. G. Minimally Augmented Karlsruhe Basis Sets. *Theor. Chem. Acc.* **2011**, *128* (3), 295–305. https://doi.org/10.1007/s00214-010-0846-z.
(65) Jorge, F. E.; Martins, L. S. C.; Franco, M. L. All-Electron Double Zeta Basis Sets for the Lanthanides: Application in Atomic and Molecular Property Calculations. *Chem. Phys. Lett.* **2016**, *643*, 84–88. https://doi.org/10.1016/j.cplett.2015.11.013.
(66) Neese, F.; Wennmohs, F.; Becker, U.; Riplinger, C. The ORCA Quantum Chemistry Program Package. *J. Chem. Phys.* **2020**, *152* (22), 224108. https://doi.org/10.1063/5.0004608.
(67) Neese, F. Software Update: The ORCA Program System—Version 5.0. *WIREs Comput. Mol. Sci.* **2022**, *12* (5), e1606. https://doi.org/10.1002/wcms.1606.
(68) Neese, F.; Wennmohs, F.; Hansen, A.; Becker, U. Efficient, Approximate and Parallel Hartree-Fock and Hybrid DFT Calculations. A 'Chain-of-Spheres' Algorithm for the Hartree-Fock Exchange. *Chem. Phys.* **2009**, *356*, 98–109. https://doi.org/10.1016/j.chemphys.2008.10.036.
(69) Shiery, R. C.; Cooper, K. A.; Cantu, D. C. Computational Prediction of All Lanthanide Aqua Ion Acidity Constants. *Inorg. Chem.* **2021**, *60* (14), 10257–10266. https://doi.org/10.1021/acs.inorgchem.1c00662.
(70) Vogel, A. I. *Vogel's Textbook of Quantitative Inorganic Analysis : Including Elementary Instrumental Analysis*; London ; New York : Longman, 1978.
(71) Pace, C. N.; Vajdos, F.; Fee, L.; Grimsley, G.; Gray, T. How to Measure and Predict the Molar Absorption Coefficient of a Protein. *Protein Sci. Publ. Protein Soc.* **1995**, *4* (11), 2411–2423. https://doi.org/10.1002/pro.5560041120.
(72) Supkowski, R. M.; Horrocks, W. DeW. On the Determination of the Number of Water Molecules, q, Coordinated to Europium(III) Ions in Solution from Luminescence Decay Lifetimes. *Inorganica Chim. Acta* **2002**, *340*, 44–48. https://doi.org/10.1016/S0020-1693(02)01022-8.

(73) Hübler, C. SupraFit – An Open Source Qt Based Fitting Application to Determine Stability Constants from Titration Experiments. *Chemistry–Methods* **2022**, *2* (7), e202200006. https://doi.org/10.1002/cmtd.202200006.
(74) Gutenthaler, S. M.; Tsushima, S.; Steudtner, R.; Gailer, M.; Hoffmann-Röder, A.; Drobot, B.; Daumann, L. J. Lanmodulin Peptides – Unravelling the Binding of the EF-Hand Loop Sequences Stripped from the Structural Corset. *Inorg. Chem. Front.* **2022**, *9* (16), 4009–4021. https://doi.org/10.1039/D2QI00933A.
(75) Alasadi, E. A.; Choi, W.; Chen, X.; Cotruvo, J. A. J.; Baiz, C. R. Lanmodulin's EF 2–3 Domain: Insights from Infrared Spectroscopy and Simulations. *ACS Chem. Biol.* **2024**, *19* (5), 1056–1065. https://doi.org/10.1021/acschembio.3c00789.
(76) Verma, G.; Hostert, J.; Summerville, A. A.; Robang, A. S.; Garcia Carcamo, R.; Paravastu, A. K.; Getman, R. B.; Duval, C. E.; Renner, J. Investigation of Rare Earth Element Binding to a Surface-Bound Affinity Peptide Derived from EF-Hand Loop I of Lanmodulin. *ACS Appl. Mater. Interfaces* **2024**, *16* (13), 16912–16926. https://doi.org/10.1021/acsami.3c17565.
(77) Shiery, R. C.; Fulton, J. L.; Balasubramanian, M.; Nguyen, M.-T.; Lu, J.-B.; Li, J.; Rousseau, R.; Glezakou, V.-A.; Cantu, D. C. Coordination Sphere of Lanthanide Aqua Ions Resolved with Ab Initio Molecular Dynamics and X-Ray Absorption Spectroscopy. *Inorg. Chem.* **2021**, *60* (5), 3117–3130. https://doi.org/10.1021/acs.inorgchem.0c03438.
(78) D'Angelo, P.; Zitolo, A.; Migliorati, V.; Chillemi, G.; Duvail, M.; Vitorge, P.; Abadie, S.; Spezia, R. Revised Ionic Radii of Lanthanoid(III) Ions in Aqueous Solution. *Inorg. Chem.* **2011**, *50* (10), 4572–4579. https://doi.org/10.1021/ic200260r.
(79) Habenschuss, A.; Spedding, F. H. The Coordination (Hydration) of Rare Earth Ions in Aqueous Chloride Solutions from X-ray Diffraction. III. SmCl3, EuCl3, and Series Behavior. *J. Chem. Phys.* **1980**, *73* (1), 442–450. https://doi.org/10.1063/1.439895.
(80) Hu, A.; MacMillan, S. N.; Wilson, J. J. Macrocyclic Ligands with an Unprecedented Size-Selectivity Pattern for the Lanthanide Ions. *J. Am. Chem. Soc.* **2020**, *142* (31), 13500–13506. https://doi.org/10.1021/jacs.0c05217.

TOC Graphic